Available online at www.sciencedirect.com
SCIENCE DIRECT®
Physica C 385 (2003) 49–65
PHYSICA C
www.elsevier.com/locate/physc

Electronic structure, electron–phonon coupling, and multiband effects in MgB_2

I.I. Mazin [a,*], V.P. Antropov [b]

[a] Code 6391, Naval Research Laboratory, 4555 Overlook Avenue, Washington, DC 20375, USA
[b] Ames Laboratory, Ames, IA 50011, USA

Is there anything of which one can say: "Look! This is something new"? It was here already, long ago; it was here before our time.

Ecclesiastes, 1:10

Abstract

We review the current situation in the theory of superconducting and transport properties of MgB_2. First principle calculations of the electronic structure and electron–phonon coupling are discussed and compared with the experiment. We also present a brief description of the multiband effects in superconductivity and transport, and how these manifest themselves in MgB_2.

Keywords: Band theory; Electron–phonon interaction; Multi-gap superconductivity

1. Introduction

Many of us remember that fabulous excitement that reigned in physics world after the discovery of high-T_c cuprates. Since then, we have become so familiar with record-breaking temperatures of 90, 120, and 160 K, that it is worth recalling that 15 years ago not only the highest known superconducting temperature was meager 24 K, but it was also believed by many since early 70's [1] that this temperature is close to the theoretical limit for electron–phonon superconductivity.

High-T_c superconductivity revolutionized our approaches both to theory and to experiment. However, in the shadow of mysterious cuprates lower-temperature superconductors were receiving relatively little attention.

This has been changed recently. In 2001 alone, besides the report of 40 K superconductivity in the simple magnesium diboride, exciting cases of superconductivity coexisting with magnetism ($ZrZn_2$), possibly induced by magnetism (ε-Fe), or competing with magnetism ($MgCNi_3$) were reported. While all these cases are different and probably manifest quite different physics, all of them indicate that the physics community turned its face back to low-temperature superconductivity. And, of course, MgB_2 is the champion of the year, hands down.

* Corresponding author. Tel.: +1-202-767-6990; fax: +1-202-404-7546.

0921-4534/02/$ - see front matter
PII: S0921-4534(02)02299-2

Very similar to the high-T_c cuprates, immediately after its discovery [2] some authors described MgB_2 as an extreme case of conventional, "Eliashberg" superconductivity, an extremely lucky combination of the fortunate parameters [3,4], while the others suggested variety of exotic electronic mechanisms, possibly similar to cuprates [5–9]. But the analogy stops here. Now, two years after the discovery, we already have much better understanding and much more universal consensus about the physics of MgB_2, than about cuprates. In fact, an agreement emerges that it is, albeit still an electron–phonon superconductor, a case of genuinely novel physics, sufficiently unusual to set it apart from all previous electron–phonon superconductors [10].

One of the main factors that distinguishes MgB_2 apart from the high-T_c cuprates is that the electronic structure of this materials is very well described by conventional band-theoretical methods, which have been perfected in the last decades to the level that allows unprecedentally detailed first-principle calculations of electron and phonon spectra, and of the electron–phonon calculations. Excellent agreement of such ab initio calculations with the experiment literally leaves hardly any room to play with exotic, but hardly verifiable models, so popular in the high-T_c world. In this chapter we will try to present a broad view on the physics of MgB_2, as it currently emerges from the first-principle calculation, and seems to be fully supported by the experiment.

The chapter is organized as follows: The electronic structure of bulk MgB_2 is discussed in Section 2, which also deals with some experiments that give credit to the calculated band structure. In Section 3 we discuss first principles calculations of the phonon spectra and the electron–phonon coupling (EPC). Section 4 is devoted to the discussion of multiband effects in MgB_2.

2. Electronic structure

2.1. General description

MgB_2 occurs in the AlB_2 structure. Boron atoms reside in graphite-like (honeycomb) layers stacked with no displacement [11] forming hexagonal prisms with the base translation almost equal to the height, $a = 3.085$ (3.009) Å and $c/a = 1.142$ (1.084) for MgB_2 (AlB_2). These prisms contain large, nearly spherical pores occupied by Mg atoms. This structure may therefore be regarded as that of completely intercalated graphite [12] with carbon replaced by boron, its neighbor in the periodic table. Furthermore, MgB_2 is formally isoelectronic to graphite. Therefore, chemical bonding and electronic properties of MgB_2 are expected to have some similarity to those of graphite and graphite intercalation compounds, some of which also exhibit superconductivity. As in graphite ($R_{intra} = 1.42$ Å), the intralayer B–B bonds are much shorter than the interlayer distance, and hence the B–B bonding is strongly anisotropic. However, the intralayer bonds are only twice as short as the interlayer ones, compared to the ratio of 2.4 in graphite, allowing for a significant interlayer hopping. For comparison, the interatomic distance between nearest neighbors is 1.55 Å in diamond and 1.4–1.45 Å in the C_{60} molecule.

In spite of a structural similarity to intercalated graphite and, to some extent, to doped fullerenes, MgB_2 has a qualitatively different and rather uncommon structure of the conducting states setting it aside from both these groups of superconductors. The peculiar and (so far) unique feature of MgB_2 is the incomplete filling of the two σ bands corresponding to strongly covalent, sp^2-hybrid bonding within the graphite-like boron layer. The holes at the top of these σ bands manifest notably two-dimensional properties and are localized within the boron sheets, in contrast with mostly three-dimensional electrons and holes in the π bands, which are delocalized over the whole crystal. These 2D covalent and 3D metallic-type states contribute almost equally to the total density of states (DOS) at the Fermi level, while the unfilled covalent bands experience strong interaction with longitudinal vibrations in the boron layer.

The band structure of MgB_2 had been reported long before the discovery of superconductivity [13–16] and is now known in very detail. The results discussed in this chapter were obtained using LMTO-ASA, full-potential LMTO, or full-poten-

tial LAPW method. Computational details may be found in respective original publications. For MgB_2, there is usually little difference between different methods, in any event, none important for the qualitative discussions in this chapter.

The energy bands, DOS and the Fermi surface of MgB_2 are shown in Figs. 1–3. As expected, the bands are quite similar to those of graphite with three bonding σ bands corresponding to in-plane sp_xp_y (sp^2) hybridization in the boron layer and two π bands (bonding and antibonding) formed by

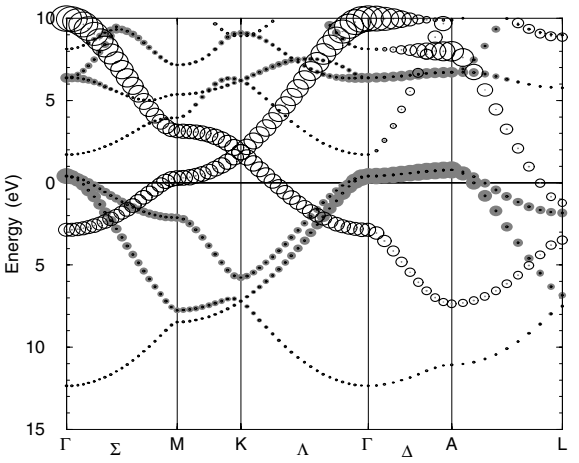

Fig. 1. Band structure of MgB_2 with the B p-character. The radii of the hollow (filled) circles are proportional to the π (σ) character.

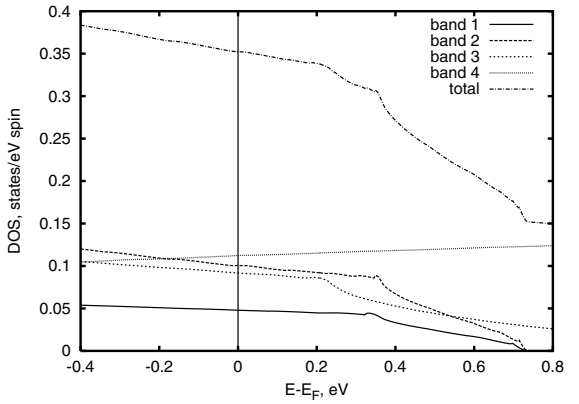

Fig. 2. Total DOS and partial DOS for MgB_2. Bands 1, 2 are σ bands, bands 3, 4 are π bands.

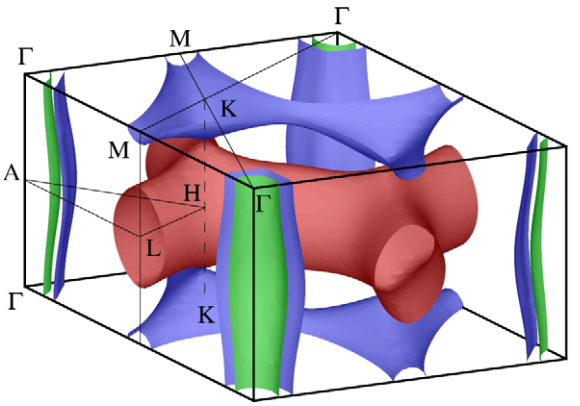

Fig. 3. Fermi surface of MgB_2.

aromatically hybridized boron p_z orbitals. Both σ and π bands have strong in-plane dispersion due to the large overlap between all p orbitals (both in-plane and out-of-plane) for neighboring boron atoms. The interlayer overlaps are much smaller, especially for p_{xy} orbitals, so that the k_z dispersion of σ bands does not exceed 1 eV. On the other hand, in contrast to intercalated graphites, two of the σ bands are filled incompletely. Together with weak k_z dispersion this results in the appearance of two nearly cylindrical sheets of the Fermi surface (see Fig. 3) around the Γ–A line. As we will see below from the analysis of the charge density (CD) distribution, these unfilled σ bands with boron p_{xy} character fully retain their covalent structure. Conducting covalent bonds represent a peculiar feature of MgB_2 making it an exotic compound probably existing on the brink of structural instability.

It is seen in Fig. 3 that the π bands form two planar honeycomb tubular networks: an antibonding electron-type sheet centered at $k_z = 0$ (red) and a similar, but more compact, bonding hole-type sheet centered at $k_z = \pi/c$ (blue). These two sheets touch at some point on the K–H line. The hole-type sheet is close to an electronic topological transition at the M point corresponding to the breakdown of the tubular network into separate starfish-like pockets (at 0.25 eV above E_F).

In order to examine the relation between the band structure of MgB_2 and that of graphite in more detail one can compare the following hypothetical sequence of intermediate materials: carbon

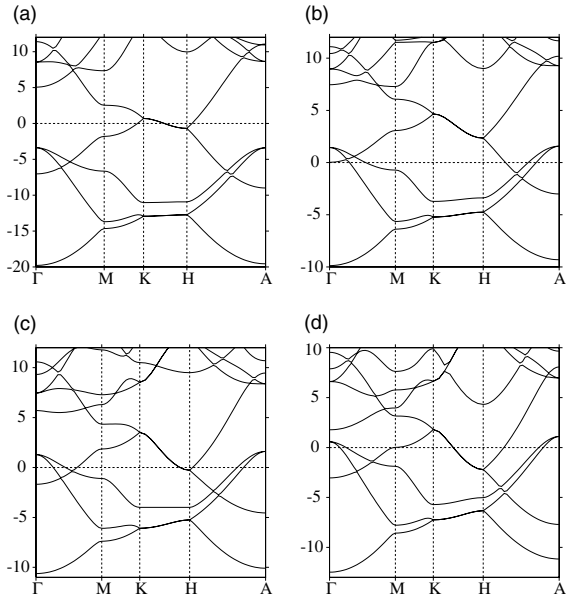

Fig. 4. Band structures of: (a) top left: primitive (AA stacking) graphite (PG), $a = 2.456$ Å, $c/a = 1.363$; (b) top right: PG boron, $a = 3.085$ Å, $c/a = 1.142$ (as in MgB_2); (c) bottom left: LiB_2 in MgB_2 structure, same a and c/a; (d) bottom right: MgB_2, same a and c/a. Energy is in eV relative to E_F. The order of occupied bands in the Γ point is σ bonding with boron s-character, π bonding with boron p_z character, and σ bonding with boron p_{xy} character (double degenerate).

in the 'primitive graphite' (PG) lattice with no displacement between layers as in MgB_2, using graphite lattice parameters; boron in the PG lattice with a as in MgB_2 and c/a as in graphite; boron in the PG lattice with a and c/a as in MgB_2; LiB_2 in the same structure; MgB_2 itself. The results of some of these calculations [17,18] are shown in Fig. 4.

The band structure of PG carbon shown in Fig. 4a is very similar to that of graphite [19] with the appropriate zone-folding for a smaller unit cell. (This is quite natural because of the weak interlayer interaction.) Boron in the same lattice (not shown) has nearly identical bands with the energies scaled by the inverse square of the lattice parameter, in agreement with canonical tight-binding scaling [20]. Fig. 4b shows the natural enhancement of the out-of-plane dispersion of the π bands when the interlayer distance is reduced. Fig. 4c and d demonstrate that 'intercalation' of boron by Li or Mg produces a significant distortion of the band structure, so that the role of the intercalant is not simply donating electrons to boron's bands (which would recover the band structure of PG carbon shown in Fig. 4a). The main change upon intercalation is the downward shift of the π bands compared to σ bands. For Li this shift of $\sim$1.5 eV is almost uniform throughout the Brillouin zone. Replacement of Li by Mg shifts the π bands further, but this shift is strongly asymmetric increasing from $\sim$0.6 eV at the Γ point to $\sim$2.6 eV at the A point. In addition, the out-of-plane dispersion of the σ bands is also significantly enhanced. In LiB_2 the filling of the bonding p_{xy} bands is nearly the same as in PG boron, while in MgB_2 the Fermi level shifts closer to the top of these bands.

The lowering of the π bands in MgB_2 compared to PG boron is due to stronger interaction of boron p_z orbitals with ionized magnesium sublattice compared to p_{xy} orbitals. This lowering is greater at the AHL plane compared to the ΓKM plane, because the antisymmetric (with $k_z = \pi/c$) overlap of the boron's p_z tails increases the electronic density close to the magnesium plane where its attractive potential is the strongest.

The nature of bonding in MgB_2 may be understood from the CD plots [18] shown in Fig. 5. As it is seen in Fig. 5a, bonding in the boron layer is typically covalent. The CD of the boron atom is strongly aspherical, and the directional bonds with high CD are clearly seen (see also Ref. [16]). The CD distribution in the boron layer is very similar to that in the carbon layer of graphite [19]. This directional in-plane bonding is also obvious from Fig. 5b showing the CD in the cross section containing both Mg and B atoms. However, Fig. 5b also shows that a large amount of valence charge does not participate in any covalent bonding, but is rather distributed more or less homogeneously over the whole crystal. Further, Fig. 5c shows the difference of the CD of MgB_2 and that of hypothetical NaB_2 in exactly the same lattice. Not only does it show that one extra valence electron is not absorbed by boron atoms but that it is rather delocalized in the interstitials; it also shows that some charge moves away from the boron atoms and covalent in-plane B–B bonds. Fig. 5d shows the CD difference between the isoelectronic com-

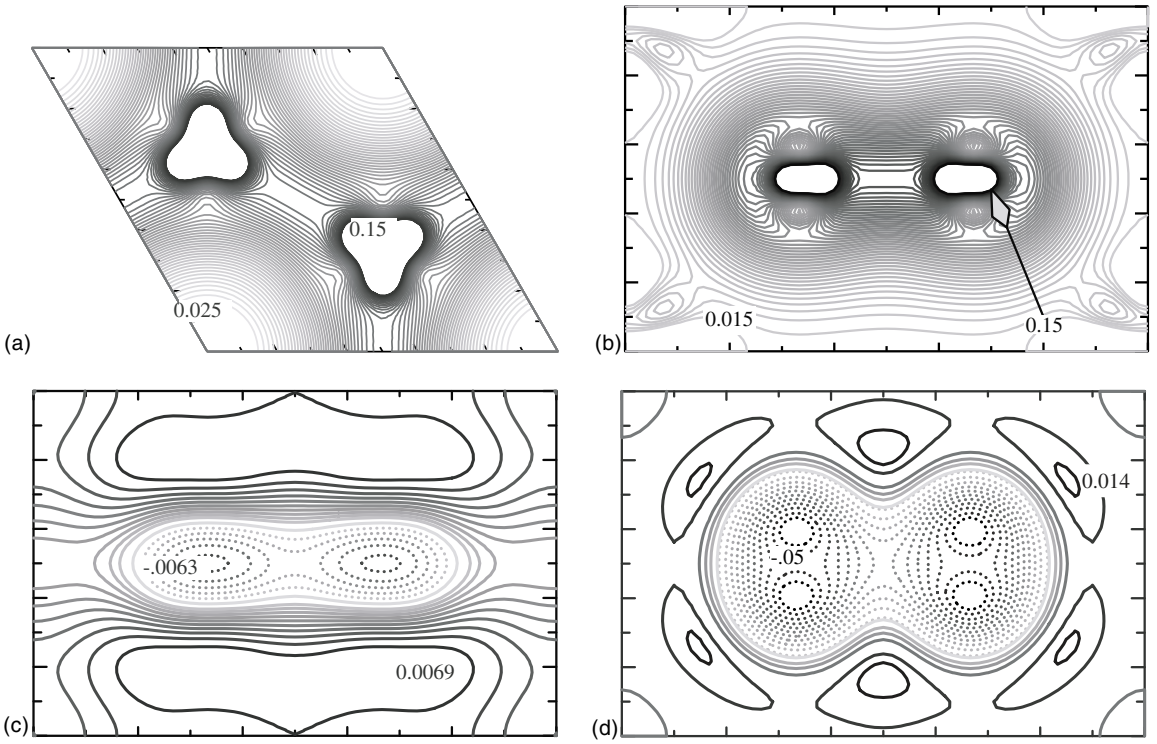

Fig. 5. Pseudocharge density contours obtained in FLMTO. The unit cell is everywhere that of MgB_2. Darkness of lines increases with density. (a) MgB_2 in (0 0 0 2) plane passing through B nuclei; (b) MgB_2 in (1 0 0 0) plane passing through Mg nuclei at each corner of the figure. B nuclei occupy positions (1/3, 1/2) and (2/3, 1/2) in the plane of the figure. The integrated charge of the unit cell is 8. (c) (1 0 0 0) plane, difference in smoothed density, MgB_2 minus NaB_2. The integrated charge of the unit cell is 1. (d) (1 0 0 0) plane, difference in smoothed density, MgB_2 minus PG carbon. The integrated charge of the unit cell is 0. In (c) and (d), dotted lines show negative values.

pounds MgB_2 and PG carbon (C_2). In MgB_2, the electrons see approximately the same external potential as in C_2, except that one proton is pulled from each C nucleus and put at the Mg site. It is evident that the change $C_2 \rightarrow MgB_2$ weakens the two-center σ bonds (the charge between the atoms is depleted) and redistributes it into a delocalized, metallic density.

A numerical reconstruction of the electronic CD from the synchrotron radiation data for a powder MgB_2 sample [21] supports this general picture. The CD found for 15 K is, in fact, very similar to that in Fig. 5b and shows all the important features discussed above including the distinct covalent bonds within the boron sheets, the strongly ionized Mg, and the delocalized charges in the interstitials. Further, the Fourier maps obtained [11] for the single crystals also clearly show the covalent sp^2 hybrids in the boron layer and no covalent bonding between B and Mg atoms.

Thus, one can say that MgB_2 is held together by strongly *covalent* bonds within boron layers and by delocalized, '*metallic*-type' bonds between these sheets. A peculiar feature of this compound is that electrons participating in both of these bond types provide comparable contributions to N. This distinguishes MgB_2 from closely related graphites where covalent bonds in the carbon layers are always completely filled, while the nearly cylindrical parts of the Fermi surface commonly found in those compounds are formed by carbon-derived π bands which are much less 3D that the corresponding bands in MgB_2 [22].

Because of the coexistence of two different types of conducting states, one needs to see the contributions to the total DOS and transport properties

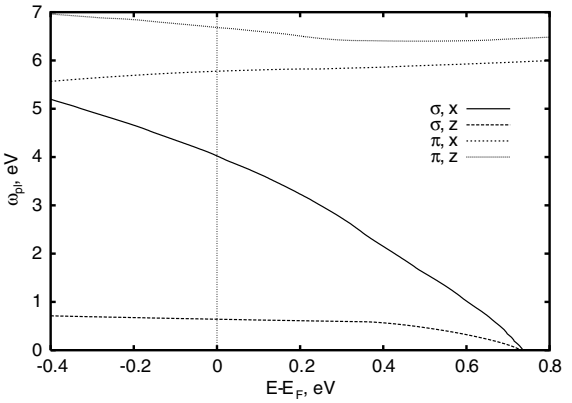

Fig. 6. Plasma frequencies for σ and π bands.

from separate sheets of the Fermi surface originating from 2D covalent and 3D metallic-type bonding. This decomposition is shown in Fig. 2 for the DOS and in Fig. 6 for the in-plane (xx) and out-of-plane (zz) components of the plasma frequency $\omega^2_{\mathrm{pl}\,\alpha} = (e^2/2\pi^2)\int v^2_\alpha \delta[\epsilon(\mathbf{k}) - E_\mathrm{F}]\,\mathrm{d}\mathbf{k}$, where v_α is the α component of the Fermi velocity. The 3D (metallic-type bonding) and cylindrical (covalent bonding) parts of the Fermi surface contribute, respectively, about 58% and 42% to $N(E_\mathrm{F})$. If the σ Fermi surfaces were ideal cylinders, $N(E_\mathrm{F})$ for these bands would have a step-like singularity at some 0.5 eV above E_F. This is broadened by a nonzero z-dispersion. The hole π band has a 3D van Hove singularity in the same range of energies, while the electron-like π band has a DOS which is rather flat around E_F. π bands contribute about 80% to the total ω^2_{pl}, and thus, given the same relaxation rate for all bands, to total conductivity. While the total conductivity is more or less isotropic, the σ band conductivity is, as expected, highly anisotropic.

2.2. Experimental probes of electronic structure

It is well known that in some materials conventional band structure calculations do not reproduce the experimental one-electron excitation spectra with sufficient accuracy. These case usually involve strongly correlated materials (cuprates, heavy fermions, etc.) with localized d- or f-electrons. On the first glance, MgB_2 does not seem to belong to any of such classes. However, it was important to verify experimentally how reliable are LDA calculations in this compound.

One of the most popular experimental probes of electronic band structure is angular-resolved photoemission spectroscopy (ARPES), particularly in view of remarkable progress achieved in the last decade. In spite of the fact that ARPES probes only a very thin surface layer and is therefore not always representative of the bulk electronic structure, first experiments [23] show an exceptional agreement between the theory and the experiment in the whole studied energy range. Both σ bands and π band were observed along the ΓM direction, as predicted by the calculations. Along ΓK direction only one out of the two predicted σ bands was observed; the authors speculated that the single experimental feature in this region may result from the superposition of the two bands. On the other hand, the fact that the band in question has different symmetry along the two measured directions may contribute to the selection rules. In addition, the analysis of the electronic states centered around the Γ point revealed that this feature originated from a surface electronic state, which is in good overall agreement between APRES and theoretical results for the Mg-terminated surface [24]. Unfortunately, to the best of our knowledge, surfaces with partial Mg coverage, say, 50%, were not studied theoretically, although this is the most likely termination. Possibly even better agreement can be achieved if such termination will be included in the calculations.

A classical probe of the Fermi surface properties are quantum oscillations, e.g., de Haas-van Alphen (dHvA) effect. Such measurements have been reported [25]. Three dHvA frequencies were clearly resolved in data from Ref. [25], corresponding to two distinct sheets of the Fermi surface. A comparison of the calculated frequencies [26–28] with the experimental data shows excellent agreement. The discrepancies with the theory are less than 300 T which is only 0.2% of the area of the hexagonal BZ. The detailed angular dependence of F_1, F_2, and F_3 has been calculated in Ref. [26] and compares favorably with the experimental results. The ratio of experimental and theoretical

effective masses provides mass renormalization, presumably of electron–phonon origin, which appears to be 1.08–1.2 for the inner σ cylinder and 0.40 for the π sheet. This is to be compared with the calculated numbers of 1.25 [10], 1.57 [29], ~1.1 [30], and 0.47 [10], 0.50 [29], ~0.33 [30]; a rather good agreement. Overall, ARPES and dHvA experiments, taken together, fully support LDA calculations, leaving hardly any room for many body renormalization of the band masses and velocities, apart from the EPC renormalization.

It is worth noting that for the π orbit it was possible to estimate the local Stoner enhancement factor. It appears that LDA calculations underestimate the exchange splitting induced by a magnetic field by about 50%. The reason for this discrepancy is not clear yet. On the other hand, electron spin resonance measurements [31,32] found electronic spin susceptibility of $(2.0–2.3) \times 10^{-5}$ emu/mol, corresponding to a Stoner renormalization of 50% less than calculated [33,34].

Since both ARPES and DHVA spectroscopy in MgB_2 are described in detail in other chapters of this book, we shall refer the reader to those, and will concentrate in the following on another probe of the electronic structure near the Fermi level, namely nuclear magnetic resonance (NMR).

NMR spectroscopy measures two electronic structure related quantities, the Knight shift, K, and the spin–lattice relaxation rate, $1/T_1T$. The former is related to the uniform spin susceptibility, the latter to the local susceptibility at a nucleus. Both are linked to the DOS at the Fermi level, but in an indirect way involving hyperfine interactions. Therefore extracting reliable information about the electronic structure is usually possible only if the corresponding calculations of the hyperfine field are available.

For MgB_2, this is the case. Several experimental groups reported $1/T_1T$ [35–37] and K for the B site [36,37], which is of particular interest because of the role that B states play in superconductivity. Two groups reported first principles calculations for $1/T_1T$ [33,34] and for K [34]. Importantly, it appears that NMR in MgB_2 not only probes B electrons, but it also probes differently σ and π bands. Indeed, since σ bands are formed by the p_x and p_y states, they can form $p_x \pm p_y$ combinations, which have nonzero orbital moment. One can therefore expect considerable orbital contribution to the relaxation rate. Indeed, calculations show [33,34] that the orbital mechanism dominates over the two others, the Fermi-contact and the spin-dipolar, mechanisms in the spin–lattice relaxation. On the contrary, for the Mg nucleus the dominant relaxation mechanism is, as usually, the Fermi-contact interaction, which also dominates the B and Mg Knight shift [34].

The results of the calculations agree well with the experiment. The experimental numbers for $1/T_1T$ on ^{11}B are in a range of $(5.6–6.1) \times 10^{-3}$/K s. Calculations using bare susceptibility produce numbers of 5.1×10^{-3}/K s [33] and 3.7×10^{-3}/K s [34]. This numbers are subject to many body renormalization. Renormalized values involve additional assumptions; in Ref. [33] the renormalized relaxation rate was estimated to be 8.1×10^{-3}/K s, while Ref. [34] gives a range of $(4.3–5.9) \times 10^{-3}$/K s. As regards the Knight shift, unfortunately, the spread of the experimentally obtained values is still too large to allow for a quantitative comparison with the calculations.

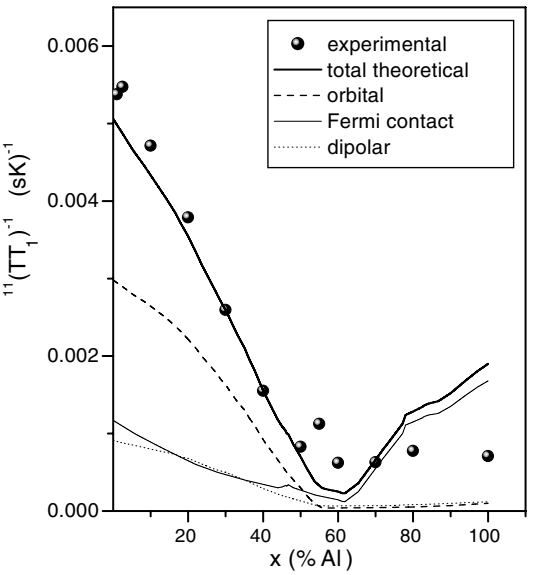

Fig. 7. Boron $^{11}(1/T_1T)$ for $Mg_{1-x}Al_xB_2$ as a function of Al-doping. Lines show the ab initio calculated plots from Refs. [17,18].

As mentioned above, the NMR relaxation rate is very sensitive to the relative amount of σ and π states, which implies a nontrivial dependence on the filling of the σ bands. This was indeed calculated in Ref. [18] for MgB_2 doped with Al (whose primary effect is to fill σ hole states). In Ref. [38] the theoretically predicted in Ref. [18] tendencies were experimentally verified for the entire $Mg_{1-x}Al_xB_2$ system of alloys. Very impressive agreement was obtained (Fig. 7).

3. Electron–phonon coupling

3.1. Standard formulas

Standard description of the EPC in metals is sometimes referred to as Migdal–Eliashberg theory. We are not going to review this theory here, as it can be found in many excellent texts, but will briefly remind the basic formulas of this theory. The primary notion of this formalism is that of the linear EPC vertex, $g_{\mathbf{k},\mathbf{k}+\mathbf{q},\nu} = \langle \mathbf{k}|\mathrm{d}V/\mathrm{d}Q_{\mathbf{q},\nu}|\mathbf{q}\rangle$, where $\mathrm{d}V/\mathrm{d}Q_{\mathbf{q},\nu}$ is the derivative of the crystal potential with respect to the normal phonon coordinate. $\mathbf{k}$, $\mathbf{k}+\mathbf{q}$ stand for the electron wave vectors, and $\mathbf{q}$, ν for the wave vector and the mode index of the phonon whose interaction with the electrons is being described. In other words, $g_{\mathbf{k},\mathbf{k}+\mathbf{q},\nu}$ is the probability of an electron to be scattered from the state $|\mathbf{k}\rangle$ into the state $|\mathbf{k}+\mathbf{q}\rangle$ by the phonon $(\mathbf{q},\nu)$. The Migdal theorem (which holds for MgB_2) states that this vertex is not renormalized by higher order processes. It does not state, however, as discussed below, that anharmonic corrections to the phonon spectra or nonlinear vertices like $\langle \mathbf{k}|\mathrm{d}^2V/\mathrm{d}Q^2_{\mathbf{q},\nu}|\mathbf{k}+\mathbf{q}\rangle$ are necessarily negligible.

$g_{\mathbf{k},\mathbf{k}+\mathbf{q},\nu}$, if properly integrated over all possible virtual electron–hole pairs, defines the phonon self-energy. In particular, its imaginary part, the phonon line width, is given by

$$\gamma_{\mathbf{q},\nu} = 2\pi\omega_{\mathbf{q},\nu}\sum_{\mathbf{k}}|g_{\mathbf{k},\mathbf{k}+\mathbf{q},\nu}|^2\delta(\varepsilon_{\mathbf{k}}-E_{\mathrm{F}}) \times \delta(\varepsilon_{\mathbf{k}+\mathbf{q}}-\varepsilon_{\mathbf{k}}-\hbar\omega_{\mathbf{q},\nu}).$$

In this formula, the right-hand side does not explicitly depend on $\omega_{\mathbf{q},\nu}$ (the prefactor cancels the corresponding factor in $|g_{\mathbf{k},\mathbf{k}+\mathbf{q},\nu}|^2$). Sometimes a related quantity, the EPC constant for a given mode, is used: $\lambda_{\mathbf{q},\nu} = \gamma_{\mathbf{q},\nu}/\pi N(E_{\mathrm{F}})\omega^2_{\mathbf{q},\nu}$. One may note that this quantity is strictly zero for optical zone center ($\mathbf{q}=0$) phonons; however, a related constant can be introduced, $\lambda^{ZZ}_{\nu} = [2N(E_{\mathrm{F}})/\omega_{\nu}]\times\sum_{\mathbf{k}}|g_{\mathbf{k},\mathbf{k},\nu}|^2$, and $g_{\mathbf{k},\mathbf{k},\nu}$ is obviously related to the deformation potential.

When integrated over all phonon modes and corresponding intermediate electron states, $g_{\mathbf{k},\mathbf{k}+\mathbf{q},\nu}$ defines the electron self-energy, or mass renormalization $(m^*/m)_{\mathbf{k}}$:

$$\left(\frac{m^*}{m}\right)_{\mathbf{k}} - 1 = \sum_{\mathbf{q},\nu}\frac{2}{N(E_{\mathrm{F}})\omega_{\mathbf{q},\nu}}|g_{\mathbf{k},\mathbf{k}+\mathbf{q},\nu}|^2 \times \delta(\varepsilon_{\mathbf{k}}-E_{\mathrm{F}})\delta(\varepsilon_{\mathbf{k}+\mathbf{q}}-\varepsilon_{\mathbf{k}}-\hbar\omega_{\mathbf{q},\nu}).$$

Finally, when integrated over all phonons with given frequency and over electronic states at the Fermi level, it defines the EPC spectral function, which determines superconducting properties of a single-gap superconductor,

$$\alpha^2F(\omega) = \frac{1}{2}\sum_{\mathbf{q},\nu}\omega_{\mathbf{q},\nu}\lambda_{\mathbf{q},\nu}\delta(\omega-\omega_{\mathbf{q},\nu})$$

which can be broken into $n\times n$ matrix separating the interband pairing interaction from the intraband one

$$\alpha^2F(\omega)_{ij} = (1/N_i(E_{\mathrm{F}}))\sum_{\mathbf{q},\nu}\sum_{\mathbf{k}\in i,\mathbf{k}+\mathbf{q}\in j}|g_{\mathbf{k},\mathbf{k}+\mathbf{q},\nu}|^2 \times \delta(\varepsilon_{\mathbf{k}+\mathbf{q}}-\varepsilon_{\mathbf{k}}-\hbar\omega_{\mathbf{q},\nu})\delta(\omega-\omega_{\mathbf{q},\nu}),$$

where i, j label different electronic bands or group of bands, e.g., $i=\sigma,\pi$.

3.2. First principle calculations

In the first publication [3] following the discovery of SC in MgB_2 the strength of the EPC was estimated and it was suggested that MgB_2 is a standard BCS superconductor, where coupling with the B phonons is the driving force for superconductivity. A substantial B, but small Mg isotope effects were predicted. Both predictions were confirmed by the experiment [39,40]. The relevant phonons were soon identified in Ref. [4] as two optical E_{2g} modes, which was confirmed by subsequent full-scale calculations of EPC.

Because of pronounced dissimilarity between different electron groups and different phonon

Table 1
Electron–phonon calculations and selected calculations of other relevant parameters, as reported in the literature

	$\omega_{E_{2g}}^{harm}$ (cm^{-1})	$\omega_{E_{2g}}^{anharm}$ (cm^{-1})	ω_{log} (cm^{-1})	$N(E_F)$ (st./Ry spin)	λ^{harm}	λ^{anharm}
Ref. [29]	540[a]		504	4.83	0.87	
Ref. [41]	536		487		0.73	
Ref. [10]			450	4.83	0.77	0.70
Ref. [30]	506	612	479	4.83	0.73	0.61
FPLAPW [10]	536[a]	590		4.80		

[a] Updated results with a better k-point convergence (J. Kortus, private communication).

modes it is unavoidable for understanding superconductivity in MgB_2 to calculate EPC spectral function $\alpha^2F(\omega)$ including all bands and all phonons on the same footing. By now, at least four groups have claimed to have done this from the first principles [10,29,30,41]. Three of these [10,30,41] were based on pseudopotential band structure calculations; one [29] utilized a full-potential LMTO method. Three used the linear response formalism to compute phonon spectra and electron–phonon matrix elements [10,29,41]; one [30] was based on frozen phonon calculations at several high-symmetry point with a subsequent interpolation onto a finer mesh. The last work also used an anharmonic correction to the phonon frequencies, which the other three works did not include (Ref. [10] provided a rough estimate of the effect). The results are compared in Table 1, and the E_{2g} frequencies are compared with selected frozen phonon calculations.

The last two columns in Table 1 show *isotropic*, or thermodynamic EPC constant; as discussed later, it is probably not directly relevant to superconductivity, but it defines the average electronic mass renormalization, and thus the renormalization of specific heat. The latest experiments [42–44] (the latter two on single crystals), reported for the electronic specific heat coefficient the values of $\gamma = 2.5$, 2.3, and 3.5 mJ/mol K^2, respectively (the discrepancy may be partially related to different temperature ranges used in fitting). The unrenormalized DOS (Table 1) corresponds to $\gamma = 1.67$ mJ/mol K^2, yielding λ from 0.4 to 1.1. While clearly inconclusive, these numbers are equally consistent with all entries in Table 1.

As regards the EPC there is a noticeable discrepancy between different calculations, despite an overall agreement. Part of that may be due to different band structure techniques, but the difference is too large to be ascribed to the band structure difference alone (note nearly perfect agreement between the calculated DOS in Table 1). At least part of the difference comes from the difference in the calculated phonon frequencies. Direct calculations of the phonon frequencies by the frozen–phonon technique are generally more reliable and less sensitive to the the size of the basis set than linear response methods. All electron calculations are usually more reliable than pseudopotential calculations. Therefore we included in the table the results of full-potential LAPW calculations. In view of high sensitivity to the phonon spectra, the fact that only a handful of high-symmetry points were treated from the first principles in Ref. [30] is a weak point of this work.

However, the differences in the phonon spectra do not explain the discrepancy in the value of the calculated EPC constants. To understand where this discrepancy possibly originates, let us note that if the σ band Fermi surfaces were ideal cylinders (which they nearly are), the EPC for the E_{2g} phonons would have two Kohn-like divergencies. [1] Indeed, it is easy to show that in this case the partial EPC constant for a E_{2g} phonon with a wave vector q, λ_q, is given by the expression

$$\lambda_q \approx \frac{\langle g^2 \rangle}{2\pi E_F \omega_q x \sqrt{1-x^2}},$$

where $\langle g^2 \rangle$ is the average EPC matrix element, $\omega_q \approx \omega_0$ is the phonon frequency, and $x = q/2k_F$.

[1] In principle, near such a singularity the Migdal theorem is violated and one has to solve the Dyson equation for the phonons self-consistently (O.V. Dolgov, unpublished). However, since these singularities are integrable it is not important for us at the moment.

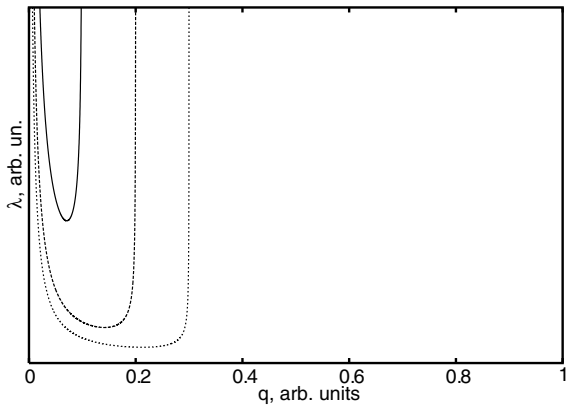

Fig. 8. Dependence of the partial EPC constant on the phonon wave vector for a cylindrical Fermi surface. Note singularities at small q and at $q = 2k_F$. Three curves correspond to three different k_F, but all integrate to the same total λ.

Note that λ_q is inversely proportional to the Fermi energy, and therefore to the number of phonons with $q < 2k_F$, so that the total λ given by the sum over all E_{2g} phonons does not depend on the size of the Fermi surface. This is, of course, simply a reflection of the fact that the DOS of a 2D band does not depend on the Fermi energy, and the total λ is, essentially, just total DOS times the average squared EPC matrix element.

This function is plotted in Fig. 8. Essentially, in the calculations like Refs. [10,29,30,41] one needs either to integrate these singularities numerically or apply to them a special analytical treatment. The first approach was employed in Refs. [29,30,41]. In particular, in Ref. [29] a special care was taken to assure that the singularity was properly integrated. In Ref. [10] the small q singularity was treated analytically; but not the high-q one. Later estimates [I.I. Mazin, unpublished] show that the discrepancy between Refs. [29] and [10] is substantially reduced when the high-q singularity is treated analytically as well, although the total λ remains slightly smaller that in Ref. [29].

3.3. Phonon renormalization, anharmonicity, and nonlinear coupling

In this section we will address several seemingly unrelated, but in fact strongly connected issues. As mentioned above, calculated frequencies of the E_{2g} phonon show strong anharmonicity [30]. At the same time, calculations show this phonon to soften abruptly around $q < 2k_F$, where k_F is the Fermi vector for the σ bands [29,41]. Finally, it was noticed that the matrix elements for quadratic EPC, $g^{quad} = \langle|\delta^2 V/\delta Q^2|\rangle$ are anomalously large compared with that for the linear coupling, $g^{lin} = \langle|\delta V/\delta Q|\rangle$ [10,45].

To understand these effects we should recall that in the linear coupling regime the effect of the electronic screening on the phonon self-energy (Fig. 9, top) is defined by the same process that determines the contribution of the corresponding phonon to the total superconduction EPC constant. Indeed, the imaginary part of the phonon self-energy (phonon line width) is related to λ_q as $\gamma_q = \pi N(E_F)\omega_q^2\lambda_q$. At the same time, the real part of the same self-energy defines phonon softening. Only the phonons with $q < 2k_F$ can couple with the σ electrons, therefore they and only they become screened and softened by them. For a zone-center phonon, there is a quantitative measure of this softening [46]:

$$\Delta\omega^2 = -4\omega\langle g^2\rangle N(E_F), \tag{1}$$

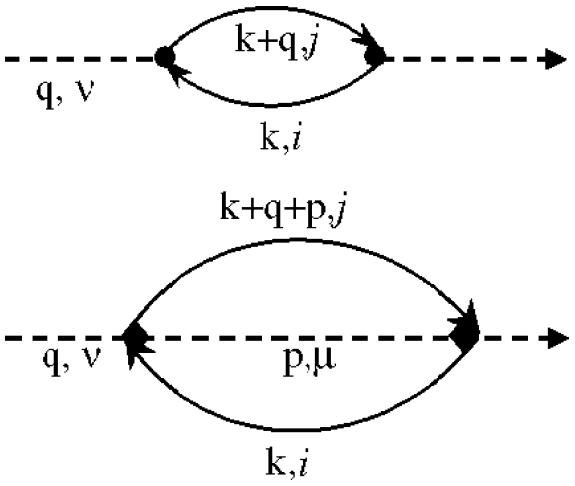

Fig. 9. Examples of the processes contributing to the phonon self-energy in the linear (top) or quadratic (bottom) approximations for the EPC.

where the right-hand side does not depend on ω. This quantity was calculated in Ref. [10] to be [2] approximately $2 \times 0.51\omega^2 \approx 1.02 \times 503^2$ cm^{-2}. This corresponds to a bare frequency of 715 cm^{-1}. In the same work, the frequency of the E_{2g} phonon away from the Γ point was calculated to be around 640 cm^{-1}. Softening from 715 to 640 cm^{-1} must therefore be coming from the screening due to the π electrons. Given high sensitivity of phonon frequencies to the k-mesh convergency, one can probably say that first principle calculations give a softening due to σ electrons of 75–100 cm^{-1}.

Eq. (1) is based on the linear approximation, that is, EPC is proportional to the first derivative with respect to the phonon coordinate. This is, however, not an easily justifiable approximation in case of MgB_2: as we saw above, the second-order EPC vertex, g^{quad}, is anomalously large. In this case one has to consider in the phonon renormalization processes corresponding to creation/annihilation of an electron–hole pair, associated with emission/absorption of two E_{2g} phonons, as illustrated in Fig. 9 (bottom). Note that the corresponding diagrams are temperature dependent, therefore producing intrinsically anharmonic phonons, as observed in the frozen phonon calculations. Quadratic EPC is a long known phenomenon (see, e.g., Refs. [47–49]), although most authors concentrated on its effect on superconductivity and mass renormalization, rather than on phonon frequencies.

In order to gain a better insight into the interrelation between the anharmonicity, quadratic coupling, and frozen phonons, let us look for the reason for the anomalously large quadratic vertex. One can conveniently write the dispersion of the two σ bands as $\epsilon_{\mathbf{k}} = u_{\mathbf{k}} \pm v_{\mathbf{k}}$, where both u and v are quadratic functions of k, and $v = 0$ at $k = 0$. The function u describes the average dispersion neglecting hybridization between the two bands, while v describes the hybridizations. Both functions depend on the frozen phonon coordinate, but in a different way: for a given point $\mathbf{k}$, u is an odd function of the phonon coordinate, $\mathrm{d}u_{\mathbf{k}}/\mathrm{d}Q \neq 0$; however, any symmetry lowering increases hybridization between the two σ bands, therefore v is an even function of Q, $\mathrm{d}v_{\mathbf{k}}/\mathrm{d}Q = 0$, $\mathrm{d}^2v_{\mathbf{k}}/\mathrm{d}Q^2 \neq 0$. At the Γ point $\mathrm{d}u/\mathrm{d}Q = 0$, therefore only nonlinear coupling remains; when going away from the Γ point, a nonzero linear component appears (which is responsible for a large calculated EPC in Refs. [10,29,30,41]), and quadratic coupling gradually vanishes. Correspondingly, the smaller is the number of holes in the σ band the stronger are anharmonic effects in the phonon frequency.

The same can be seen from the point of view of the frozen phonon calculations. These amount to calculating total energy of a crystal with fixed ionic displacement comparable with, or smaller than the amplitude of the zero-point oscillations. This energy remains more or less harmonic as long as the frozen displacement does not incur any change in the Fermi surface topology. This "critical" displacement becomes smaller when the σ-pockets get filled, therefore yielding more and more anharmonic phonons, in perfect agreement with the reasoning above.

The interrelated nonlinearity and anharmonicity have competing effects on superconductivity. Anharmonic hardening of the phonon reduces effective EPC constant (Table 1), while two-phonon exchange provides an additional contribution to $\alpha^2F(\omega)$ at frequencies roughly twice the frequency of the E_{2g} phonon. The latter effect was never reliably calculated. Estimates of Yildirim et al. [45] allow one to assume that nonlinear EPC increases the coupling constant for σ bands by at least 5%, although this is probably the lower estimate.

4. Multiband effects in superconductivity

Already in the first months after the discovery of superconductivity in MgB_2 experiments appeared that were not consistent with a conventional strong coupling superconductivity scenario. It was observed that the critical field [50], specific heat [51] and tunneling [52] measurements are easier to explain if two gaps are assumed instead of one. Liu et al. [10] proposed, based on electronic structure and EPC calculations, that there are, in fact, two distinctive gaps associated with σ- and

[2] The value reported for λ_{ZZ} in Ref. [10] was $\approx$0.6; it was later refined to be 0.51 (A.Y. Liu, private communication).

Table 2
2×2 EPC matrices in different calculations

Ref. [10]		Ref. [53]		Ref. [30][a]	
0.96	0.17	1.02	0.16	0.78	0.11
0.23	0.29	0.21	0.45	0.15	0.21

[a] Obtained by integrating $\lambda(\mathbf{k},\mathbf{k}')$ distribution plots from Ref. [30].

π-Fermi surfaces. This "two-gap" model gained popularity, and it became clear that the EPC calculations needed to be performed separately for the two sets of bands.

With this in mind, the results of Ref. [10] and subsequently of Ref. [29] were broken in a 4×4 EPC matrix, as well as in a 2×2 matrix (Table 2). Ref. [30] does not report the corresponding 2×2 matrix, but it can be reasonably accurately restored from the figures in that paper. Detailed calculations [30] show that in the ideally clean limit the variation of the order parameter, apart from the $\sigma - \pi$ difference, are less than 10%. As discussed below, such a variation cannot exist in real sample even with an extremely small impurity concentration, therefore it is of little interest to use more than 2×2 EPC matrix in any physically relevant discussion.

4.1. General theory

The famous BCS formula is derived in the assumption that the pairing amplitude (superconducting gap, order parameter) is the same at all points on the Fermi surface. The variational character of the BCS theory makes one think that giving the system an additional variational freedom of varying the order parameter over the Fermi surface should always lead to a higher transition temperature. This problem was solved first in 1959 by Matthis and coworkers [54] and by Moskalenko [55]. The general solution was given later by several authors (probably in the most developed form by Allen and Mitrovich [56]), and for our purpose can be written as

$$\Delta(\mathbf{k}) = \int \Lambda(\mathbf{k},\mathbf{k}')\Delta(\mathbf{k}')F[\Delta(\mathbf{k}'),T]\,\mathrm{d}\mathbf{k}', \tag{2}$$

where summation over $\mathbf{k}$ implies also summation over all bands crossing the Fermi level. The matrix Λ characterizes the electron–phonon interaction, and the temperature dependence is given by the function

$$F = \int_0^{\omega_D} \mathrm{d}E \tanh\left(\left(\sqrt{E^2+\Delta^2}\right)\Big/2T\right)\Big/\sqrt{E^2+\Delta^2}.$$

For the purpose of this paper it suffices to use the discrete (also called disjoint) representation, where it is assumed that the order parameter Δ varies little within each sheet of the Fermi surface, while differing between the different sheets:

$$\Delta_i = \sum_j \Lambda_{ij}\Delta_j F(\Delta_j, T), \tag{3}$$

where i, j are the band indices and Λ is an *asymmetric* matrix related to the *symmetric* matrix of the pairing interaction, $\Lambda_{ij} = V_{ij}N_j$, where N_i is the contribution of the ith band to the total DOS. It can be shown that in the BCS weak coupling limit the critical temperature is given by the standard BCS relation, $kT_c = \hbar\omega_D \exp(-1/\lambda_{\mathrm{eff}})$, where λ_{eff} is the largest eigenvalue of the matrix Λ. The ratios of the individual order parameters are given by the corresponding eigenvector. Note that although the matrix Λ is not symmetric, its eigenvalues are the same as those of the symmetric matrix $\sqrt{N}V\sqrt{N}$.

The mass renormalization parameters for each band can be constructed from the matrix Λ: $\lambda_i = \sum_j \Lambda_{ij}$. These λ_i define, among other things, the dHvA thermal masses. Finally, the renormalization of the specific heat is given by the weighted average of λ_i, $\bar{\lambda} = \sum_i N_i\Lambda_{ij}/N_{\mathrm{tot}} = \sum_{ij} N_i\Lambda_{ij}N_j/N$, which is also the "Eliashberg" coupling constant determining the superconductivity in the isotropic limit, where all order parameters are constrained to be the same. One can show that $\bar{\lambda} \leqslant \lambda_{\mathrm{eff}}$, the equality being achieved when and only when all elements of the V matrix are the same (the relative magnitude of N_i is irrelevant). Physically this result is obvious: the BCS theory can be formulated as a variational theory. Therefore a bigger energy gain, and a higher critical temperature, can be achieved if more variational freedom is provided, e.g., by allowing different order parameters in the different bands.

4.2. Impurity scattering

In this section we will outline nontrivial effects related to impurity scattering in a multigap superconductor. The discussion will mostly follow Ref. [57], where more details can be found. In the Born approximation, and close to T_c, the problem can be solved analytically. It appears that nonmagnetic impurities suppress superconductivity in much the same way, as magnetic ones do in a regular superconductor, however, only the interband impurity scattering has a pair-breaking effect. In the weak nonmagnetic scattering limit, for two bands, the T_c suppression is

$$\frac{\delta T_c}{T_c} = -\frac{\pi\gamma_{12}}{8kT_c}\frac{(\Delta_1-\Delta_2)(\Delta_1 N_2-\Delta_2 N_1)}{(\Delta_1^2+\Delta_2^2)N_2}, \tag{4}$$

where $\gamma_{12}\equiv\gamma_{21}N_2/N_1$ is the interband scattering rate. Note that the T_c suppression is linear in γ_{12}. This formula also gives us a clue about what is a weak and what is a strong scattering in the specific case of MgB_2: small scattering is when $\gamma_{12}\ll(\delta\Delta^2/\bar{\Delta}^2)T_c$, where $\delta\Delta$ is the variation of the gap between the bands, and $\bar{\Delta}$ is the average gap. The ratio of the σ and the π band gaps is, experimentally and theoretically, of the order of 3. The densities of states are comparable. Therefore a T_c suppression of 1 K would require an interband scattering rate of the order of 1 meV. It is a fortunate and rather unexpected coincidence that the symmetry of the electronic states conspire in such a way as to make the interband scattering rate quite small even in rather dirty samples [58]. Only because of this conspiracy we are actually able to observe two distinctive gaps in this compound.

On the other hand, the variation of the gap within each of the two-band systems, calculated in Ref. [30], which is of the order of 7%, cannot survive a σ–σ impurity or phonon scattering stronger than $\sim$0.01 meV, and therefore is unobservable in samples of any imaginable quality.

In the strong interband scattering limit a complete isotropization of all Fermi surfaces takes place. This limit is achieved [57] when the interband scattering rate becomes larger than the relevant phonon frequency, in our case, 600 $cm^{-1}\approx$ 75 meV. Then the two gaps merge to one, the isotropic BCS gap, and the critical temperature drops to it isotropic value. Strong coupling calculations of Ref. [30] predict the latter to be around 19 K. Indeed, recent experiments on irradiated samples [59] demonstrated a reduction of the gap ratio by 40%, accompanied by a T_c reduction by 22%. One should note, however, that the results of Ref. [59], while qualitatively consistent with the prediction of the two-band model, quantitatively do not agree with them. Similar results were reported in Ref. [60].

4.3. Strong coupling and Coulomb pseudopotential

It is relatively straightforward to extend the theory of multiband superconductivity beyond the weak coupling BCS model [56]. Qualitatively one can easily understand the main effect of the strong coupling by recalling the McMillan equation:

$$kT_c = \frac{\hbar\omega_{\log}}{1.2}\exp\left[\frac{-1.02(1+\lambda)}{\lambda-\mu^*(1+0.62\lambda)}\right]. \tag{5}$$

Qualitatively, this equation can be understood as renormalized BCS equation, $kT_c=\hbar\omega_{ph}\exp[-1/(\lambda-\mu^*)]$, where $\omega_{ph}=\omega_{\log}/1.2$, and the mass renormalization has been applied to λ, $\lambda\to\lambda/(1+\lambda)$. We already know that the multiband version of the BCS equation differs from this in that λ is substituted by an effective λ_{eff}, the largest eigenvalue of the matrix Λ. The effect of Coulomb repulsion, introduced in the BCS model via the Coulomb pseudopotential μ^*, is likewise introduced in its multiband version via the *matrix* μ^*_{ij}. The multiband analog of the McMillan equation is, therefore,

$$kT_c = \frac{\hbar\omega_{\log}}{1.2}\exp\left[\frac{-1}{(\lambda-\mu^*)_{\rm eff}}\right], \tag{6}$$

where $(\lambda-\mu^*)_{\rm eff}$ is defined as the maximum eigenvalue of the matrix

$$\Lambda^{\rm eff}_{ij} = \frac{\Lambda_{ij}-\mu^*_{ij}(1+0.62\sum_n\Lambda_{in})}{1+\sum_n\Lambda_{in}}. \tag{7}$$

This expression gives the results very close to the full solution of the multiband Eliashberg equations.

The Coulomb pseudopotential matrix is not a constant, as it is sometimes believed [30]. First of all, already the *bare* pseudopotential matrix, μ_{ij}, is not uniform. Indeed, it is formally defined as $\langle\langle V_C\rangle\rangle_{ij}N_j$ (where V_C is the screened Coulomb interaction, and the averaging is over the corresponding Fermi surfaces), and as had been noticed, for instance, by Agtergerg et al. in another compound [61], when different bands have different orbital character, the Coulomb matrix elements between these bands are suppressed compared to intraband matrix elements. Jepsen and Andersen [62] estimated this effect, using the tight-binding LMTO method and found the ratio between $\langle\langle V_C\rangle\rangle_{\sigma\sigma}$, $\langle\langle V_C\rangle\rangle_{\pi\pi}$ and $\langle\langle V_C\rangle\rangle_{\sigma\pi}$ to be ≈3:1.8:1. Furthermore, any anisotropy in *bare* pseudopotential is further enhanced in the renormalized μ^*_{ij}. In the one-band case μ is renormalized as $\mu^* = [\mu/(1+\mu\log(W/\omega_{\log}))]$, where W is a characteristic electronic frequency (of the order of the bandwidth or plasma frequency). For a multiband case we have a matrix equation, which is a natural extension of the standard procedure [63]

$$\mu^*_{ij} = \mu_{ij} - \sum_n \mu_{in}\log(W_n/\omega_c)\mu^*_{nj}. \tag{8}$$

It is easy to show that renormalization enhances any nonuniformity in μ; indeed, assuming $\mu_{\sigma\sigma} = \mu_{\pi\pi} = \alpha\mu_{\sigma\pi}$, $(\alpha > 1)$, and $\mu_{\sigma\sigma}\log(W_\sigma/\omega_c) = \mu_{\pi\pi}\log(W_\pi/\omega_c) = L$, we obtain $\alpha^* = \alpha + (\alpha - 1/\alpha)L$. From the ratios of $\langle\langle V_C\rangle\rangle$'s above, $\alpha \sim 2.3$, and L for MgB_2 is of the order of 0.5–1, so for μ^*_{ij} it holds that $\mu^*_{\sigma\sigma} = \mu^*_{\pi\pi} \sim 4\mu^*_{\sigma\pi}$.

The fact that the matrix μ^*_{ij} is approximately diagonal is of utmost importance. Various calculations [10,29,30] differ in details, but all agree that the interband EPC constant is 0.15–0.2. Since the order parameter in the π band is induced by the σ band (except for the very low temperature), if a Coulomb repulsion offsets most of the interband coupling, the induced gap becomes vanishingly small. If $\mu^*_{\sigma\pi}$ were of the order of $\mu^*_{ii} \approx 0.1$, the gap ratio Δ_σ/Δ_π would be much larger than the observed ratio of approximately 3. It is worth mentioning that this is in direct contradiction with a popular misconception that "the superconducting properties of MgB_2 are not very sensitive to μ^*" [30]; they are not only in the one-band picture. To demonstrate this, we performed [62] 2×2 Eliashberg calculations using the electron–phonon interaction from Ref. [30]. Although the authors of Ref. [30] do not break down their results for the EPC in a two-band form, which would have made them easier to analyze, one can find the 2×2 matrix corresponding to their calculations by integrating the $\lambda(\mathbf{k},\mathbf{k}')$ distribution depicted in their graphs (Table 2). It appeared that with $\mu^*(\omega_c) = 0.12$, used in Ref. [30], the ratio Δ_σ/Δ_π at zero temperature is 5.5 and the critical temperature $T_c = 43$ K. On the other hand, calculations with a *diagonal* matrix, $\mu^*_{\sigma\pi} = 0$, $\mu_{\sigma\sigma} : \mu_{\pi\pi} = N_\sigma : N_\pi$, produced $T_c = 38$ K and $\Delta_\sigma/\Delta_\pi = 3.6$.

4.4. Normal transport

A closer look at normal transport in MgB_2 reveals several phenomena which are hard to understand. First, there is a severe violation of the Matthiessen rule: samples with large residual resistivity tend to have much stronger temperature dependence of the resistivity than "clean" samples. Second, optical conductivity does not seem to obey the Drude–Lorenz law; if one attempts a Drude–Lorenz fit to experimental spectra, the extracted plasma frequency is five times smaller than expected. Many researchers believe that these problems are due to extrinsic effects like grain boundaries. While future experiments will clarify this matter, it interesting to observe that multiband effects can actually explain such observations rather easily.

The theory of multiband effects in electric transport has been developed by Allen and coworkers [64]. One important qualitative statement can be made upfront: since the kinetic equation in a metal can be solved variationally with respect to the electric conductivity, giving a variational freedom for different bands to change their distribution functions separately should always result in an increase of the conductivity. In other words, while in the one-band theory the superconducting, the thermodynamic, and the transport EPC constants are usually similar (the first two being identical), in the multiband theory the former is always larger than in the corresponding one-band scenario, and the latter is always smaller. Quanti-

tatively, one can write down the following formulas:

$$\sigma = e^2 \sum_{ij} (\rho^{-1})_{ij}, \tag{9}$$

$$\rho_{ij} = t_{ij} \Big/ \left[\sum_{\mathbf{k}} v_{i\mathbf{k}}^2 \delta(\varepsilon_{i\mathbf{k}}) \right] \left[\sum_{\mathbf{k}} v_{j\mathbf{k}}^2 \delta(\varepsilon_{j\mathbf{k}}) \right], \tag{10}$$

$$t_{ij} = t_{ij}^{\text{out}} - t_{ij}^{\text{in}} \tag{11}$$

$$= \delta_{ij} \sum_{\mathbf{k}\mathbf{k}'n} P_{i\mathbf{k},n\mathbf{k}'} v_{i\mathbf{k}}^2 \delta(\varepsilon_{i\mathbf{k}}) \delta(\varepsilon_{n\mathbf{k}'}) \tag{12}$$

$$- \sum_{\mathbf{k}\mathbf{k}'} P_{i\mathbf{k},j\mathbf{k}'} v_{i\mathbf{k}} v_{j\mathbf{k}'} \delta(\varepsilon_{i\mathbf{k}}) \delta(\varepsilon_{j\mathbf{k}'}), \tag{13}$$

where $v_{i\mathbf{k}}$ is the electron velocity along the direction of the current. The physical meaning of these formulas is just that of the parallel conductors formula, each element of the matrix ρ^{-1} representing a separate conductor. If the scattering probability $P_{i\mathbf{k},j\mathbf{k}'}$ is reasonably isotropic, averaging over the Fermi surface renders t_{ij}^{in} very small. Neglecting it, and using the standard expressions for the phonon-limited and impurity parts of $P_{i\mathbf{k},j\mathbf{k}'}$, we have, for two bands,

$$1/\rho_{\text{DC}}(T) = \frac{1}{4\pi} \left(\frac{\omega_{\text{pl}\,\pi}^2}{\Gamma_\pi(T)} + \frac{\omega_{\text{pl}\,\sigma}^2}{\Gamma_\sigma(T)} \right),$$

$$\Gamma_\sigma(T) = \gamma_{\sigma\sigma} + \gamma_{\sigma\pi} + \frac{\pi}{T} \int_0^\infty \mathrm{d}\omega \frac{\omega}{\sinh^2(\omega/2T)} \times \left[\alpha_{\text{tr}}^2(\omega) F_{\sigma\sigma}(\omega) + \alpha_{\text{tr}}^2(\omega) F_{\sigma\pi}(\omega) \right], \tag{14}$$

where the plasma frequencies are defined in their usual way for each Cartesian direction. The disparity of the two-band systems appears here in a trivial way, through different ω_{pl}^2, and in a nontrivial way, through different $\alpha_{\text{tr}}^2 F(\omega)$ and different γ. As described elsewhere in this chapter, the electron–phonon scattering is much stronger in the $\sigma\sigma$ channel that in the other channels, and the impurity scattering is essentially always small in the interband channel; furthermore, it is often much stronger in the $\pi\pi$ channel than in the $\sigma\sigma$ channel. The smallness of the interband impurity scattering is essential for the two-gap superconductivity; the sample-dependence of the *intraband* γ, especially of the $\gamma_{\pi\pi}$, is important for the understanding of the temperature dependence of the normal resistivity. Indeed, it is usually assumed that the impurity scattering is, in the first approximation, irrelevant for the temperature dependence of the resistivity. It is not necessarily true in a two-band system.

To start with, let us consider a very clean sample, $\gamma_{ij} = 0$. The in-plane conductivity at $T = 0$ is defined by both bands, but mostly by the π band, because it has a larger plasma frequency. The out-of-plane conductivity, of course, is defined by the π band only. Closer to room temperature the contribution of the σ band becomes smaller and smaller, because of the strong EPC scattering in this band. Eventually, the high-T behaviour is dominated by the π band with its small EPC constant. Temperature dependence at the high-temperature (above room temperature) is therefore weak. Let us now consider a dirty sample with $\gamma_{\pi\pi} \gg \gamma_{\sigma\sigma} \gg \gamma_{\sigma\pi}$. Because of the strong impurity scattering, π electrons contribute very little to superconductivity, so the temperature dependence is defined entirely by the EPC in the σ bands—and thus is strong. For a more detail discussion of these issues we refer the reader to the paper [58].

Similar effects are expected in optical conductivity; the relevant formulas differ from Eq. (14) only in the sense that a frequency dependence of the EPC scattering should be taken into account in the usual way, and in the first line $\Gamma_i(T)$ should be substituted by $\Gamma_i(T) - i\omega$. Nontrivial effects may be expected in the "dirty" regime [65,66] $\gamma_{\pi\pi} \gg \gamma_{\sigma\sigma} \gg \gamma_{\sigma\pi}$. In this regime the Drude peak in optical conductivity that stems from the π electrons broadens, possibly beyond recognition, and manifests itself merely as a flat background. Analyzing such a conductivity will uncover only one Drude peak, the one due to σ electrons, with a much reduced spectral weight, compared to the total plasma frequency. Moreover, if $\gamma_{\sigma\sigma} \lesssim \omega_{\text{ph}} \approx 70$ meV, where ω_{ph} is the frequency of the E_g phonon, the Drude peak is further renormalized by the EPC and its spectral weight is reduced by a factor of $(1 + \lambda)$. Further discussion can be found in Ref. [65].

5. Conclusion

MgB_2 is an unusual superconductor. It is not as far from conventional materials as high-T_c cuprates, or triplet Sr_2RuO_4. The pairing symmetry is s, the driving force is electron–phonon interaction. However, several factors distinguish MgB_2 from such more usual superconductors as Nb, Nb_3Si, or even $(B,K)BiO_3$, to name a few. The differences mainly stem from the fact that the charge carriers in MgB_2 fall into two distinctive groups: π electrons, similar to those in graphites, and σ electrons, which represent highly unusual case of covalent bands crossing the Fermi level. Only the latter group demonstrate an anomalously strong interaction, and only with two phonons with sufficiently small wave vectors.

This leads to a complex of uncommon features in the band structure, transport properties, and superconductivity. In particular, the superconducting state is characterized by two distinctively different order parameters. Special symmetry of electronic states strongly suppresses the pair scattering by impurities from one-band system to the other, thus making the two-gap superconductivity surprisingly unsensitive to sample quality. MgB_2 appears to be fairly unique, and, from our point of view, it is not very likely that this compound can be optimized by a chemical modification to raise substantially its critical temperature, as opposed, for example, to high-T_c cuprates.

Acknowledgements

In course of our work on MgB_2 we enjoyed exceedingly fruitful collaborations with outstanding researchers all over the world, whose names appear in our joint publications (Refs. [3,10,17, 18,28,33,34,58]). We particularly appreciate especially close collaborations with K.D. Belashchenko (VA) and J. Kortus (IM). We also wish to acknowledge very enlightening discussions with O.K. Andersen, A.A. Golubov, O.V. Dolgov and the experimental group at the Ames Laboratory.

VA acknowledges support from Ames Laboratory, which is operated for the U.S. Department of Energy by Iowa State University under Contract no. W-7405-82. IM acknowledges support from the Office of Naval Research, and from the Kavli Institute for Theoretical Physics, where part of this work was carried out, under the National Science Foundation grant no. PHY99-07949.

References

[1] M.L. Cohen, P.W. Anderson, Comments on the maximum superconducting temperature, in: D.H. Douglass (Ed.), Superconductivity in d- and f-Metals, AIP, New York, 1972, p. 17.
[2] J. Nagamatsu, N. Nakagawa, T. Muranaka, Y. Zenitani, J. Akimitsu, Nature 410 (2001) 63.
[3] J. Kortus, I.I. Mazin, K.D. Belashchenko, V.P. Antropov, L.L. Boyer, Phys. Rev. Lett. 86 (2001) 4656.
[4] J. An, W.E. Pickett, Phys. Rev. Lett. 86 (2001) 4366.
[5] J.E. Hirsch, Phys. Lett. A 282 (2001) 392–398.
[6] K. Voelker, V.I. Anisimov, T.M. Rice, cond-mat/0103082.
[7] G. Baskaran, Phys. Rev. B 65 (21) (2002) 212505.
[8] K. Yamaji, J. Phys. Soc. Jap. 70 (2001) 1476.
[9] F. Marsiglio, Phys. Rev. Lett. 87 (2001) 247001.
[10] A.Y. Liu, I.I. Mazin, J. Kortus, Phys. Rev. Lett. 87 (2001) 087005.
[11] S. Lee, H. Mori, T. Masui, Y. Eltsev, A. Yamamoto, S. Tajima, J. Phys. Soc. Jap. 70 (2001) 2255.
[12] J.K. Burdett, G.J. Miller, Chem. Mater. 2 (1989) 12.
[13] I.I. Tupitsyn, Sov. Phys. Solid State 18 (1976) 1688.
[14] D.R. Armstrong, P.G. Perkins, J.C.S. Faraday II 75 (1979) 12.
[15] A.J. Freeman, A. Continenza, M. Posternak, S. Massidda, in: G. Benedek (Ed.), Surface Properties of Layered Structures, Kluwer, The Netherlands, 1992.
[16] A.I. Ivanovskii, N.I. Medvedeva, Russ. J. Inorg. Chem. 45 (2000) 1234.
[17] K.D. Belashchenko, M. van Schilfgaarde, V.P. Antropov, Phys. Rev. B 64 (2001) 092503.
[18] V.P. Antropov, K.D. Belashchenko, M. van Schilfgaarde, S.N. Rashkeev, in: Studies of High Temperature Superconductors, vol. 38, 2002, pp. 91–116.
[19] H.J.F. Jansen, A.J. Freeman, Phys. Rev. B 35 (1987) 8207.
[20] W.A. Harrison, Electronic Structure and the Properties of Solids, San Francisco, 1980.
[21] E. Nishibori, M. Takata, M. Sakata, H. Tanaka, T. Muranaka, J. Akimitsu, J. Phys. Soc. Jap. 70 (2001) 2252.
[22] N.B. Brandt, S.M. Chudinov, Ya.G. Ponomarev, Modern Problems in Condensed Matter Sciences, vol. 20.1, North-Holland, Netherlands, 1988.
[23] H. Uchiyama, K.M. Shen, S. Lee, A. Damascelli, D.H. Lu, D.L. Feng, Z.-X. Shen, S. Tajima, Phys. Rev. Lett. 88 (2002) 157002.
[24] V.D.P. Servedio, S.-L. Drechsler, T. Mishonov, Int. J. Mod. Phys. B 16 (2002) 1613.

[25] E.A. Yelland, J.R. Cooper, A. Carrington, N.E. Hussey, P.J. Meeson, S. Lee, A. Yamamoto, S. Tajima, Phys. Rev. Lett. 88 (2002) 217002.
[26] H. Harima, Physica C 378–381 (2002) 18.
[27] H. Rosner, J.M. An, W.E. Pickett, S.-L. Drechsler, Phys. Rev. B 66 (2002) 024521;
S. Elgazzar, P.M. Oppeneer, S.-L. Drechler, R. Hayn, H. Rosner, Solid State Commun. 121 (2002) 99.
[28] I.I. Mazin, J. Kortus, Phys. Rev. B 65 (2002) 180510.
[29] Y. Kong, O.V. Dolgov, O. Jepsen, O.K. Andersen, Phys. Rev. B 64 (2001) 020501.
[30] H.J. Choi, D. Roundy, H. Sun, M.L. Cohen, S.G. Louie, Phys. Rev. B 66 (2002) 020513, Nature 418 (2002) 758.
[31] R.R. Urbano, P.G. Pagliuso, C. Rettori, Y. Kopelevich, N.O. Moreno, J.L. Sarrao, Phys. Rev. Lett. 89 (2002) 087602.
[32] F. Simon, A. Janossy, T. Feher, F. Muranyi, S. Garaj, L. Forro, Phys. Rev. Lett. 87 (2001) 047002.
[33] K.D. Belashchenko, V.P. Antropov, S.N. Rashkeev, Phys. Rev. B 64 (2001) 132506.
[34] E. Pavarini, I.I. Mazin, Phys. Rev. B 64 (2001) 140504.
[35] H. Kotegawa, K. Ishida, Y. Kitaoka, T. Muranaka, J. Akimitsu, Phys. Rev. Lett. 87 (2002) 127001.
[36] A. Gerashenko, K. Mikhalev, S. Verkhovskii, T. D'yachkova, A. Tyutyunnik, V. Zubkov, Appl. Magn. Reson. 21 (2001) 157.
[37] J.K. Jung, S.H. Baek, F. Borsa, S.L. Bud'ko, G. Lapertot, P.C. Canfield, Phys. Rev. B 64 (1) (2002) 012514.
[38] G. Papavassiliou, M. Pissas, M. Karayanni, M. Fardis, S. Koutandos, K. Prassides, cond-mat/0204238, 2002.
[39] S. Bud'ko, G. Lapertot, C. Petrovic, C.E. Cunningham, N. Anderson, P.C. Canfield, Phys. Rev. Lett. 86 (2001) 1877.
[40] D.G. Hinks, H. Claus, J.D. Jorgensen, Nature 411 (2001) 6836.
[41] K.-P. Bohnen, R. Heid, B. Renker, Phys. Rev. Lett. 86 (2001) 5771.
[42] Y. Wang, F. Bouquet, I. Sheikin, P. Toulemonde, B. Revaz, M. Eisterer, H.W. Weber, J. Hinderer, A. Junod, cond-mat/0208169, 2002.
[43] F. Bouquet, Y. Wang, I. Sheikin, T. Plackowski, A. Junod, S. Lee, S. Tajima, cond-mat/0207141, 2002.
[44] Y. Machida, S. Sasaki, H. Fujii, M. Furuyama, I. Kakeya, K. Kadowaki, cond-mat/0207658, 2002.
[45] T. Yildirim, O. Gulseren, J.W. Lynn, C.M. Brown, T.J. Udovic, Q. Huang, N. Rogado, K.A. Regan, M.A. Hayward, J.S. Slusky, T. He, M.K. Haas, P. Khalifah, K. Inumaru, R.J. Cava, Phys. Rev. Lett. 87 (2001) 037001.
[46] O. Rodriguez, A.I. Liechtenstein, I.I. Mazin, O. Jepsen, O.K. Andersen, M. Methfessel, Phys. Rev. B 42 (1990) 2692.
[47] J.C. Hui, P.B. Allen, J. Phys. F 4 (1974) L42.
[48] R. Heid, Phys. Rev. B 45 (1992) 5052.
[49] V.H. Crespi, M.L. Cohen, Phys. Rev. B 48 (1993) 398.
[50] S.V. Shulga, S.-L. Drechsler, H. Eshrig, H. Rosner, W.E. Pickett, cond-mat/0103154.
[51] F. Bouquet, Y. Wang, R.A. Fisher, D.G. Hinks, J.D. Jorgensen, A. Junod, N.E. Phillips, Europhys. Lett. 56 (2001) 856.
[52] E. Bascones, F. Guinea, Phys. Rev. B 64 (2001) 214508.
[53] A.A. Golubov, J. Kortus, O.V. Dolgov, O. Jepsen, Y. Kong, O.K. Andersen, B.J. Gibson, K. Ahn, R.K. Kremer, J. Phys.: Condens. Mat. 14 (2002) 1353.
[54] H. Suhl, B.T. Matthias, L.R. Walker, Phys. Rev. Lett. 3 (1959) 552.
[55] V.A. Moskalenko, Fiz. Met. Met. 4 (1959) 503.
[56] P.B. Allen, B. Mitrovic, in: F. Seitz, D. Turnbull, H. Ehrenreich (Eds.), Solid State Physics, vol. 37, Academic, New York, 1982, p. 1.
[57] A.A. Golubov, I.I. Mazin, Phys. Rev. B 55 (1997) 15146.
[58] I.I. Mazin, O.K. Andersen, O. Jepsen, O.V. Dolgov, J. Kortus, A.A. Golubov, A.B. Kuz'menko, D. van der Marel, Phys. Rev. Lett. 89 (2002) 107002.
[59] Y. Wang, F. Bouquet, I. Sheikin, P. Toulemonde, B. Revaz, M. Eisterer, H.W. Weber, J. Hinderer, A. Junod, cond-mat/0208169, 2002.
[60] R.A. Ribeiro, S.L. Bud'ko, C. Petrovic, P.C. Canfield, cond-mat/0210530.
[61] D.F. Agterberg, T.M. Rice, M. Sigrist, Phys. Rev. Lett. 78 (1997) 3374.
[62] I.I. Mazin, O.K. Andersen, O. Jepsen, A.A. Golubov, O.V. Dolgov, J. Kortus, cond-mat/0212417.
[63] J.R. Schrieffer, Theory of Superconductivity, 1964, 300pp.
[64] F.J. Pinski, P.B. Allen, W.H. Butler, Phys. Rev. B 23 (1981) 5080.
[65] A.B. Kuzmenko, F.P. Mena, H.J.A. Molegraaf, D. van der Marel, B. Gorshunov, M. Dressel, I.I. Mazin, J. Kortus, O.V. Dolgov, T. Muranaka, J. Akimitsu, Solid State Commun. 121 (2002) 479–484.
[66] E.G. Maksimov, J. Kortus, O.V. Dolgov, I.I. Mazin, Phys. Rev. Lett. 89 (2002) 129703.